Journal of Biomechanics 93 (2019) 101–110

Contents lists available at ScienceDirect

Journal of Biomechanics

journal homepage: www.elsevier.com/locate/jbiomech
www.JBiomech.com

Intermediate fenestrations reduce flow reversal in a silicone model of Stanford Type B aortic dissection ☆

Joav Birjiniuk [a,*], Ravi K. Veeraswamy [b], John N. Oshinski [a,c], David N. Ku [d,e]

[a] Wallace H. Coulter Department of Biomedical Engineering, Georgia Institute of Technology, 315 Ferst Drive, Atlanta, GA 30332-0405, United States
[b] Division of Vascular Surgery, Department of Surgery, Medical University of South Carolina, 114 Doughty Street Suite BM 654 MSC 295, Charleston, SC 29425, United States
[c] Department of Radiology and Imaging Sciences, Emory University School of Medicine, 1364 Clifton Road NE Suite D112, Atlanta, GA 30322, United States
[d] George W. Woodruff School of Mechanical Engineering, Georgia Institute of Technology, 315 Ferst Drive, Atlanta, GA 30332-0405, United States
[e] Division of Vascular Surgery, Joseph B. Whitehead Department of Surgery, Emory University School of Medicine, 1365 Clifton Road, Atlanta, GA 30322, United States

ARTICLE INFO

Article history:
Accepted 20 June 2019

Keywords:
Fluid mechanics
Aortic dissection
Hemodynamics
Vascular surgery
Cardiothoracic surgery
Vortices
4D PCMR

ABSTRACT

Pulsatile, three-dimensional hemodynamic forces influence thrombosis, and may dictate progression of aortic dissection. Intimal flap fenestration and blood pressure are clinically relevant variables in this pathology, yet their effects on dissection hemodynamics are poorly understood. The goal of this study was to characterize these effects on flow in dissection models to better guide interventions to prevent aneurysm formation and false lumen flow. Silicone models of aortic dissection with mobile intimal flap were fabricated based on patient images and installed in a flow loop with pulsatile flow. Flow fields were acquired via 4-dimensional flow MRI, allowing for quantification and visualization of relevant fluid mechanics. Pulsatile vortices and jet-like structures were observed at fenestrations immediately past the proximal entry tear. False lumen flow reversal was significantly reduced with the addition of fenestrations, from 19.2 ± 3.3% in two-tear dissections to 4.67 ± 1.5% and 4.87 ± 1.7% with each subsequent fenestration. In contrast, increasing pressure did not cause appreciable differences in flow rates, flow reversal, and vortex formation. Increasing the number of intermediate tears decreased flow reversal as compared to two-tear dissection, which may prevent false lumen thrombosis, promoting persistent false lumen flow. Vortices were noted to result from transluminal fluid motion at distal tear sites, which may lead to degeneration of the opposing wall. Increasing pressure did not affect measured flow patterns, but may contribute to stress concentrations in the aortic wall. The functional and anatomic assessment of disease with 4D MRI may aid in stratifying patient risk in this population.

1. Introduction

1.1. Current methods of management

Aortic dissection results from a tear in the wall of the aorta, allowing for aberrant flows in the original true lumen and newly created false lumen (Kumar et al., 2009). Approximately 250,000 new cases of aortic dissection are reported worldwide per annum (LeMaire and Russell, 2011). Unlike Stanford Type A dissections requiring immediate open repair, Type B dissections are confined to the descending portion of the aorta, with no involvement of the ascending segment, and do not necessitate open intervention (Clough and Nienaber, 2015). As such, beta-blocker therapy remains the foundation of treatment for patients with Type B dissection (Clough and Nienaber, 2015). Such treatment is aimed at decreasing the aortic impulse via vasodilatory as well as negative chronotropic and inotropic effects, and in so doing, decreasing the stresses on the aortic wall. While pressure control is considered a central goal for beta-blocker therapy, its effects on complex fluid flow patterns in the aorta remain unclear.

Endovascular intervention has emerged as a valuable option in the treatment of Type B dissection. Results from the INSTEAD trial, and its extension INSTEAD-XL, suggest that patients undergoing stent-graft intervention may have higher survival and event-free rates at 5 years following index evaluation (Nienaber et al., 2009; Nienaber et al., 2013). While these studies are not definitive, they demonstrate a significant difference in dilatation of the thoracic aorta between study groups, suggesting the role of stent-grafting

☆ This work was presented orally at the 2016 Vascular Research Initiatives Conference, Nashville, Tennessee, May 4, 2016, and as a poster at the 2016 Vascular Annual Meeting, National Harbor, MD, June 8–11, 2016.

* Corresponding author at: 1648 Pierce Drive NE, Atlanta, GA 30307, United States.
E-mail address: jbirjin@emory.edu (J. Birjiniuk).

https://doi.org/10.1016/j.jbiomech.2019.06.019
0021-9290/

in restoring normal aortic caliber and providing more favorable remodeling of the aorta. However, it is unclear why certain patients remain stable on medical therapy alone, while some patients undergoing endovascular intervention develop aneurysm in the long-term.

1.2. Anatomic heterogeneity and outcomes

Part of the variability in outcomes among these patients is thought to result from variations in both dissection anatomy and hemodynamics (Blount and Hagspiel, 2009; Evangelista et al., 2012). In addition, interactions between these two variables may account for unique conditions that favor aneurysmal degeneration. Thrombosis of the false lumen has been a factor of particular interest, with some studies showing benefits of false lumen thrombosis, whether or not complete (Akutsu et al., 2004; Onitsuka et al., 2004; Sueyoshi et al., 2009; Ueki et al., 2014), and others finding patients with partial thrombosis faring worse than those with a completely patent false lumen (Tsai et al., 2007). Though these studies vary in their assessment of overall thrombosis, the discordance demonstrates that anatomy may only partially explain the variability in outcomes. Aortic function, as indicated by local hemodynamics, is posited to be a useful prognostic indicator (Cheng et al., 2014a; Guzzardi et al., 2015; Casas et al., 2016; Clough et al., 2012; François et al., 2013; Hope et al., 2007).

The number of tears within the resulting intimal flap is also a known anatomic variable that has attracted attention in clinical studies. The presence of multiple tears has been associated with better patient outcomes (Tolenaar et al., 2013; Tolenaar et al., 2013; Tolenaar et al., 2013), though the mechanism for this is currently unknown. It has been suggested that the presence of such tears equalizes pressures across the two flow lumina, reducing hydrostatic pressures in the false lumen that may lead to aneurysm formation. This effect has yet to be studied in a controlled fashion, but the iatrogenic formation of such tears, a process known as fenestration, has been used in the past to achieve this outcome (Berguer et al., 2015; Williams et al., 1997). The benefit of such a procedure on aortic hemodynamics is unknown.

1.3. Objectives and hypothesis

In order to understand the role of varying tear configurations on dissection hemodynamics, we employed a silicone model of the aorta with a mobile intimal flap subjected to pulsatile, physiologic flow conditions. Using 4-dimensional phase contrast magnetic resonance (4D PCMR) imaging, we obtained full time-resolved flow fields throughout the aorta for quantification. We hypothesized that models with three and four tears, including entry tear, would exhibit less flow reversal, as calculated by reverse flow index (RFI), than those with two tears alone, as the new fenestrations will allow for more low-resistance pathways for blood flow when luminal pumping is present (Birjiniuk et al., 2017). Further, we hypothesize that increased mean arterial pressure (MAP) will leave flow patterns relatively unchanged as compared to normal MAP, as flow is dictated by spatial, as opposed to temporal, gradients in pressure.

2. Methods

Mock circulation and imaging techniques were assembled and performed as described previously (Birjiniuk et al., 2017). Briefly:

2.1. Model and imaging setup

Molds of the aorta were rapid-prototyped from segmented CT angiograms of a patient with normal aortic caliber. Silicone models of dissection of the descending aorta with internal diameter of 35 mm and a mobile intimal flap were fabricated in two separate casting steps with an intermediate mold release layer. The aortic wall ranged in thickness between 2 and 3 mm, while the intimal flap measured 0.5 mm thick. The silicone chosen possessed a nominal elastic modulus in a range of 0.5–1 MPa (Characteristic Properties of Silicone Rubber Compounds, 2018) (Supplemental Fig. 1), which is consistent with that of the native aorta, approximately 0–1 MPa (Akhtar et al., 2009; Haskett et al., 2010). Entry and exit tears spanning half of the aortic circumference were incised at prescribed locations on the lateral wall along the outer curvature of the descending aorta (Birjiniuk et al., 2017). The entry tear was located at the proximal descending aorta at the flexure of its inner curvature, with an exit tear four centimeters from the distal lip of the model, for a total dissection length of 20 cm. Linear, transverse fenestrations, approximately 2.5 cm in length, were subsequently added at locations 50% and 75% of the distance from entry to exit tear (10 and 15 cm, respectively), affording models with two, three, and four tears (Fig. 1). These models were installed in a flow loop (Fig. 2) and subjected to physiologic pulsatile flow (4 L/min) established by a custom-built positive-displacement pump (Supplemental Fig. 2). Pressures were varied between normal (140/80 mm Hg), hypertensive (180/120 mm Hg) and extreme hypertensive (220/160 mm Hg) conditions in order to

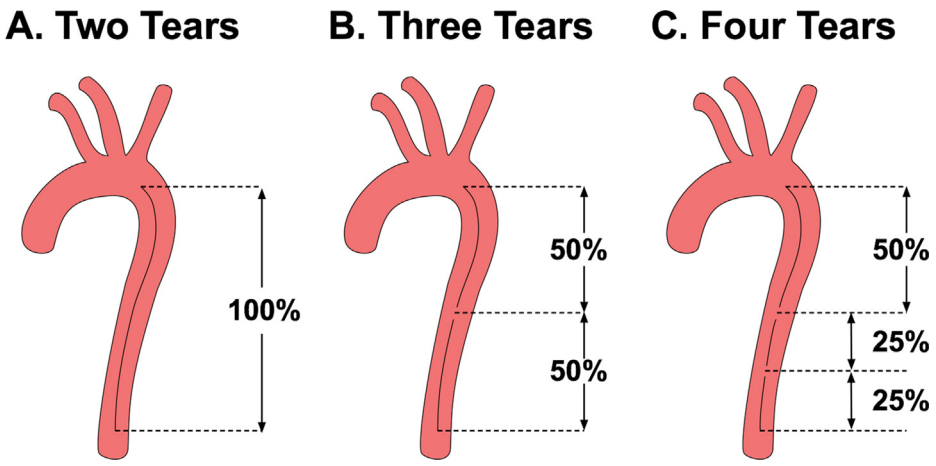

Fig. 1. Varying dissection anatomies tested with entry and exit tear only (**A**), entry, exit, and 50% flap length fenestration (**B**), and entry, exit, 50%, and 75% flap length fenestrations (**C**).

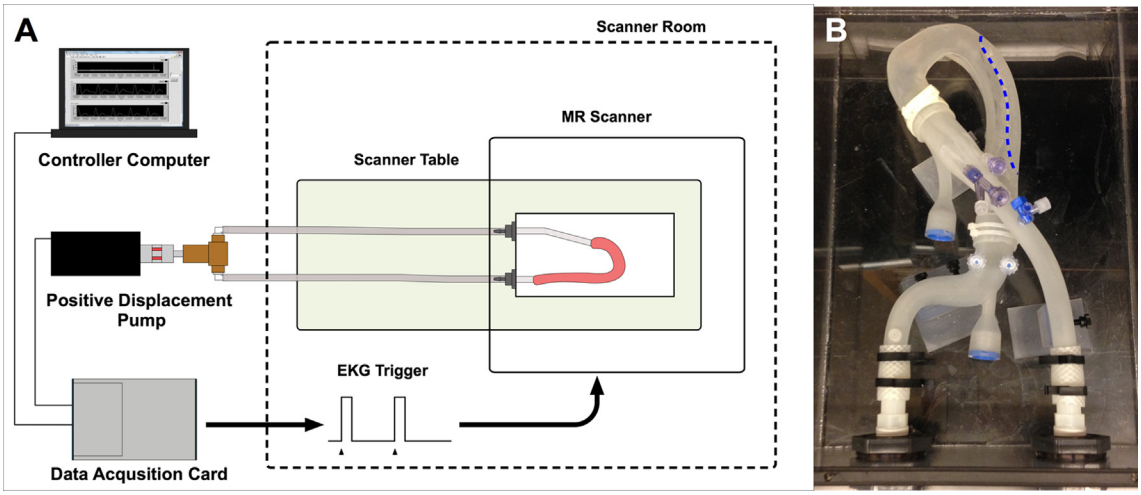

Fig. 2. Flow loop setup (A) with compliant aortic dissection model (B). The model and flow tubing are tunneled into an MRI scanner, all ferromagnetic components being shielded from the magnet. Pump drive and EKG triggering is accomplished via a data acquisition card (Reprinted with permission from: Springer Nature, *Cardiovascular Engineering and Technology*, Birjiniuk et al, "Pulsatile Flow Leads to Intimal Flap Motion and Flow Reversal in an *In Vitro* Model of Type B Aortic Dissection", 2017).

mimic pressure differences observed in patients before and after initiation of beta-blocker therapy.

Supplementary data associated with this article can be found, in the online version, at https://doi.org/10.1016/j.jbiomech.2019.06.019.

The pump apparatus and controls were left outside of the MRI scanner due to their ferromagnetic components. Rigid PVC tubing was used to connect the pump outside of the scanner to the flow loop within it. Due to the length of tubing necessary, water was chosen as working fluid in order to maintain an adequate flow rate given the power of the pump. While this limits the maximal rates of acceleration and deceleration achievable, physiologic waveforms were generated (Supplemental Fig. 2). With a heart rate of 60 beats per minute, this resulted in mean Reynolds and Womersley numbers of approximately 1630 and 17, respectively. EKG-gated 4D PCMR images (Kilner et al., 1993; Markl et al., 2012; Stalder et al., 2008) were acquired using a 3 Tesla Prisma scanner (Siemens, Erlangen, Germany) and a multi-element body surface coil. Image volumes were acquired across a field of view of 250×250 mm with 26 slices at a voxel size of $1.0 \times 1.0 \times 2.0$ mm, yielding an image volume depth of 52 mm. A velocity-encoding value of 80 cm/s in each Cartesian direction was selected to eliminate phase-wrap artifact and maximize dynamic range.

2.2. Image processing

Magnitude images were segmented semi-automatically using a level-set algorithm (MITK, Heidelberg, Germany) in order to derive lumen contours. In addition, the segmentations were used to generate volumes for computation of aortic centerlines via the Vascular Modeling Toolkit (www.vmtk.org). Segmentations, centerlines, and PCMR data were imported into custom software for phase offset correction and quantification of hemodynamics (Birjiniuk et al., 2017).

2.3. Quantification of intimal flap dynamics

Planes at the levels of entry and exit tears, as well as at distances of 25%, 50% and 75% between the entry and exit, were interrogated. The intimal flap was segmented manually throughout the cardiac cycle using the PCMR magnitude images. Coordinates along the flap were interpolated in each slice to ensure consistent numbers of points at each cardiac phase. A second spatial interpolation was performed between slices at each flap point. Thus, a constant number of points was obtained for comparison in both longitudinal and transverse spatial directions. Flap displacement was calculated as the Euclidean distance between a point on the flap at a given phase and its initial position (t = 0).

2.4. Calculation of hemodynamic parameters

Individual velocity profiles were acquired for both true and false lumen. Flow rate in each lumen was calculated by integrating the through-plane velocity at a given slice across the luminal cross-section. In-plane pixel area was corrected for the angle of the plane in absolute coordinates. Relative retrograde flow over the course of the cardiac cycle was determined by calculating the reverse flow index (Birjiniuk et al., 2017), defined as the proportion of overall blood volume flowing retrograde at a given plane in the aorta:

$$\mathrm{RFI} = 100\% \times \frac{\left|\int_0^T Q_{reverse}dt\right|}{\left|\int_0^T Q_{reverse}dt\right| + \left|\int_0^T Q_{forward}dt\right|}$$

with Q representing the flow in the subscripted direction relative to systemic circulation.

2.5. Flow visualization

Following segmentation, PCMR data was visualized in ParaView (Ahrens et al., 2005) (Kitware, Clifton Park, NY). Velocities were interpolated in time and used to generate particle paths, which were subsequently contoured for gross visualization of flow patterns. In addition, preliminary flow visualization was performed using dye injection within the model. Qualitative analysis of flow visualization was used to identify complex flows. Vortices were defined as regions in which fluid was noted to revolve around a given axis pointing in any direction within the flow.

2.6. Statistical analysis

Statistical analyses were performed using MATLAB (Mathworks, Natick, MA), with a p-value of 0.05 set as the level of significance. Continuous data are reported as mean ± standard deviation. Two-way analysis of variance (ANOVA) tests were performed at each slice in order to determine overall differences between both pres-

sure and tear-configurations. Individual one-way ANOVA tests were performed at each slice with data in opposing conditions stratified, i.e. ANOVA between tear configuration groups were performed at each pressure configuration and vice-versa. Post-hoc analysis of individual comparisons was performed with pair-wise Tukey-Kramer tests.

3. Results

3.1. Vortices localized to exit tears

Vortical structures were seen to form at the location of the exit tear in all models, the result of mixing of streams of different velocity from each lumen. With the introduction of intermediate fenestrations, additional vortices were observed to form at these sites (Fig. 3, Supplemental Videos 1 and 2). It should be noted that all of the vortices observed are right-handed with respect to the anterior-posterior axis of the aorta (Fig. 4), which is expected as a result of the skewing of the velocity profile due to the curvature of the aortic arch. It should be noted that anti-parallel (i.e. left-handed, small, and not resolved) vortices must also be formed within the flow as a consequence of the conservation of angular momentum.

3.2. Fenestrations reduce flow reversal

Fenestrations were found to reduce flow reversal as quantified by the reverse flow index when compared to dissection without intermediate tears, most notably in the proximal false lumen (Fig. 5). These results held when RFI calculations were aggregated across pressure conditions (Table 1). The prominent flow reversal in the proximal and mid-dissection false lumen of the two-tear dissection (19.2 ± 3.3%, 17.5 ± 5.7%, respectively) was significantly reduced in the three-tear (4.67 ± 1.5%, 7.05 ± 0.40%, $P < 0.001$) and four-tear dissections (4.87 ± 1.7%, 7.45 ± 2.1%, $P < 0.001$).

3.3. Transluminal fluid shift

Upon dye injection (Supplemental Video 1) and subsequent particle tracing of PCMR data (Supplemental Videos 2 and 3), fluid was observed to traverse from false to true lumen in the locale of the intermediate fenestrations (Supplemental Videos 1, 2, 3). The flow from the false lumen was noted in the change in distribution of flow between true and false lumen along the length of the dissection (Fig. 6). While relative true and false lumen flow rates remained constant along dissection with entry and exit tears only, the introduction of intermediate fenestrations led to an increase in relative true lumen flow rate longitudinally. As mass flow rate is

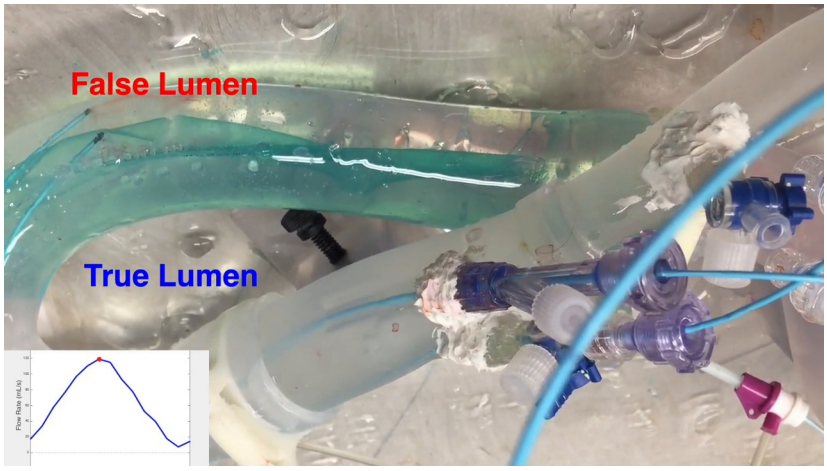

Video 1.

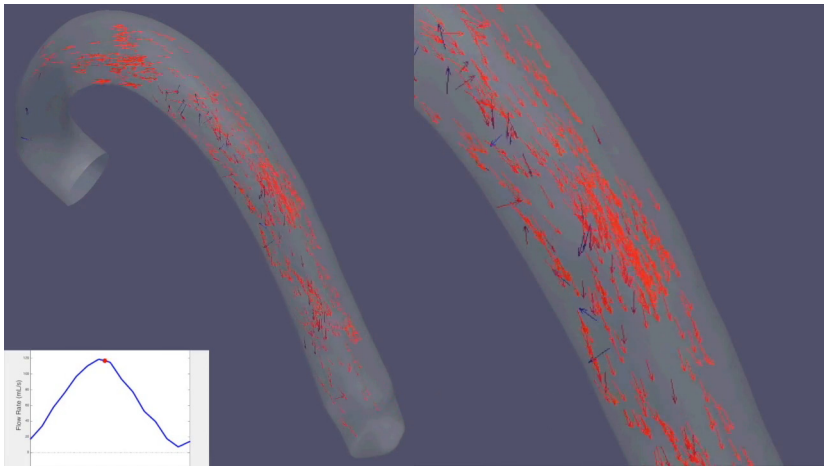

Video 2.

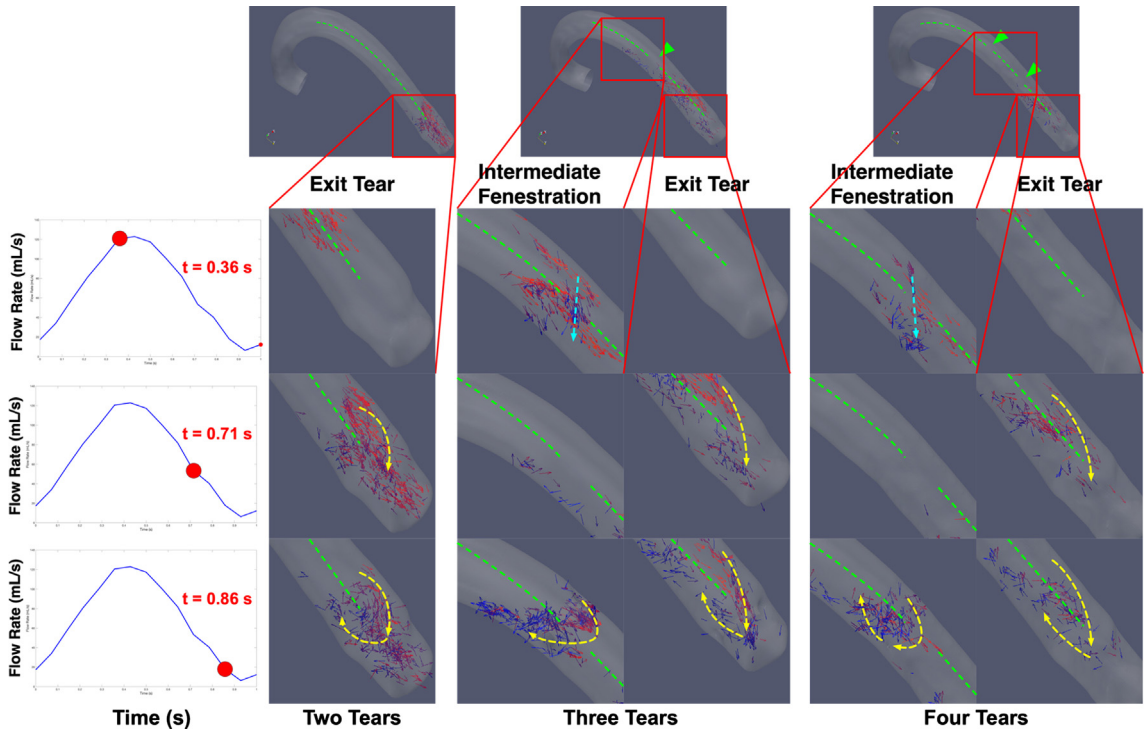

Fig. 3. Evolution of systolic jets (cyan dashed arrows) and diastolic vortices (yellow dashed arrows) at tear sites in dissections with varying number of tears. Intimal flap is outlined in green dashed line, intermediate fenestrations denoted by green arrowheads. (For interpretation of the references to colour in this figure legend, the reader is referred to the web version of this article.)

conserved, in the absence of any branch vessels, any change in relative flow rates must occur as a result of transfer of fluid from one lumen to the other. This transluminal fluid shift is also suggested by the vortices described above as the interaction of these fluid structures with true lumen flow may lead to secondary flows. Further, this appears to coincide with a qualitative decrease in forward fluid energy in the true lumen as subsequent tears are added (Supplemental Videos 1 and 2).

3.4. Conservation of flap motion and flow velocities

As with the two-tear dissection, significant motion of the intimal flap was noted in models with more fenestrations. Accentuated motion was notable at the most distal exit tear, with excursions of 14.9 ± 2.0 mm and 13.8 ± 3.8 mm at times of 0.59 ± 0.07 s and 0.66 ± 0.07 s during the cardiac period for three- and four-tear models, respectively. This action was repeated in smaller sections in which the most eccentric motion of the intimal flap was seen to occur at tear sites distal to the entry tear. At half the distance between entry and exit tear, maximal flap excursions of 13.7 ± 2.2 mm and 9.92 ± 2.5 mm at times of 0.52 ± 0.12 s and 0.54 ± 0.09 s for three- and four-tear models, respectively. In the four-tear model, a maximum excursion of 12.4 ± 3.8 mm occurred at 0.64 ± 0.10 s in the cardiac cycle at the tear located 75% of the distance between entry and exit tears.

The distal false lumen collapsed during peak systole in the fenestrated case, as with the two-tear case. This collapse may be due to the narrowing of the false lumen at this location, leading to

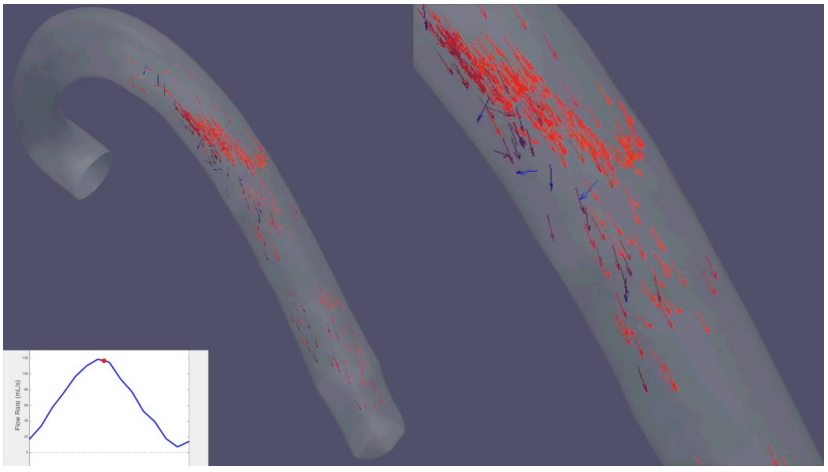

Video 3.

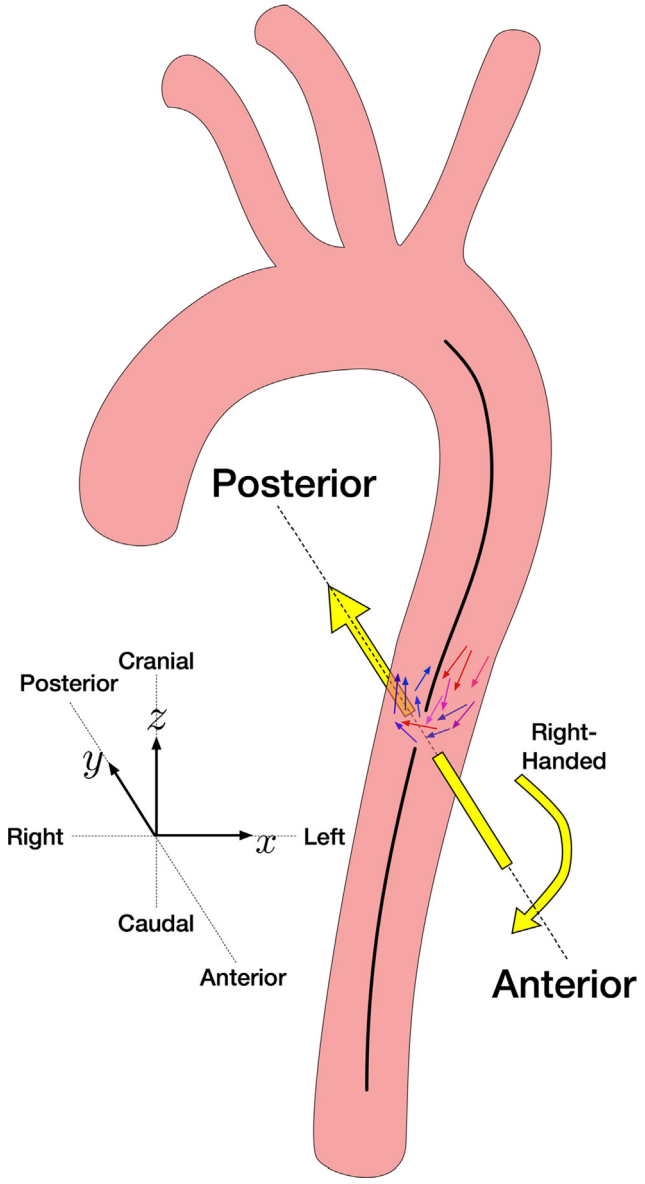

Fig. 4. Right-handed convention for describing vortices, with positive (right-handed) rotational components rotating about anterior-posterior axis.

accelerated velocities. In systole, as these velocities increase to maximum, the dynamic pressure along these streamlines decreases, which may lead to a Venturi effect, drawing in the flap to the wall of the outer aortic curvature. The approximation of the flap to the aortic wall was observed at the most distal tear only, with a patent false lumen found more proximally. Maximum velocities in both true and false lumen were consistent across varying tear configurations (Table 2).

3.5. Variations with pressure

While the fluid flow was found to vary with tear anatomy, with a given tear configuration, the vortices and flow reversals were consistent even with greater mean pressures (Fig. 5). Statistical analysis of both flow splits and RFI showed no significant differences across pressure conditions for a given tear configuration (Tables 3 and 4 respectively), save for a few individual cases ($P < 0.05$).

4. Discussion

The introduction of fenestrations between entry and exit tear was found to lead to an overall reduction in flow reversal in both true and false lumen. In addition, fluid shifts from false to true lumen were observed both qualitatively and quantitatively at tear sites. Vortices evolving in time were observed to arise at these locations as well. Absolute pressure was found not to impact flow phenomena both qualitatively and via calculation of flow rates and RFI.

As hypothesized, the fenestrations act as an alternate low-resistance pathway for fluid flow, demonstrated by the lateral fluid velocities and changes in luminal flow rates seen longitudinally along the dissection. The lateral fluid shifts across the intimal flap indicate the presence of small, localized pressure gradients developing between true and false lumen. Prior investigation revealed such structures, but did not study them in a systematic fashion (Cheng et al., 2014b; Clough et al., 2014; Karmonik et al., 2012). Further work will determine whether these structures represent true jets, which may lead to abnormal radial stresses on the opposing aortic wall upon impingement.

The interaction of this transluminal fluid at fenestration sites with flow of the opposing lumen appears to contribute to vortex formation in diastole. In this model, the excess momentum traversing from false to true lumen likely dissipates in the true lumen as clockwise vortices. Similar structures have been reported in computational and clinical study though they have been seen to occur from true to false lumen in counter-clockwise fashion (Cheng et al., 2014b; François et al., 2013). In such scenarios, these vortices may indicate lack of false lumen pressure, and may contribute to continued false lumen pressurization. The vortices seen in this model evolve over time and coincide with the pulsatile flow conditions. Time-evolving vortices of this fashion have not been reported in dissection models and may be used as a benchmark for future computational studies

In the absence of intermediate fenestrations, i.e. the two-tear configuration, any pumping action of the false lumen expels fluid retrograde as it has no other path to follow. Such flow reversals lead to oscillatory shear and potential endothelial dysfunction. In addition, they may also create stagnant regions, which could lead to false lumen thrombosis. While complete thrombosis may portend improved outcomes (Tsai et al., 2007), it is not clear how this phenomenon parlays into outcomes for patients with branch vessels supplied by the false lumen. The location of such branches, such as the left subclavian artery, relative to entry and exit tear, as well as the size of such tears, has also been shown to influence thrombosis of the false lumen (Menichini and Xu, 2016; Menichini et al., 2017). Further investigation is necessary to determine if flow reversals change disease prognosis. It is hypothesized that with the absence of retrograde flow, the false lumen in highly fenestrated dissections is less likely to thrombose. Increased fenestrations may promote sustained canalization and pressurization of the false lumen and therefore worse outcomes.

Clinically, the loss of efficiency due to flow reversal and fluid energy dissipation may lead to ischemic symptoms as a result of decreased perfusion pressure and delivered blood to end-organs. Additionally, drag induced by the resulting vortices may also contribute to left ventricular afterload. Studies of pressure and energy drops resulting from drag-inducing fluid structures and viscous interactions have contributed to understanding of ventricular afterload in aortic and valvular pathologies (Barker et al., 2014; Casas et al., 2016; Dyverfeldt et al., 2013). Thus, dissection of the descending aorta may not be a solely vascular disease, but rather have both acute and long-term consequences on the myocardium. Future study into these effects is warranted to characterize this contribution to the pathophysiology of disease.

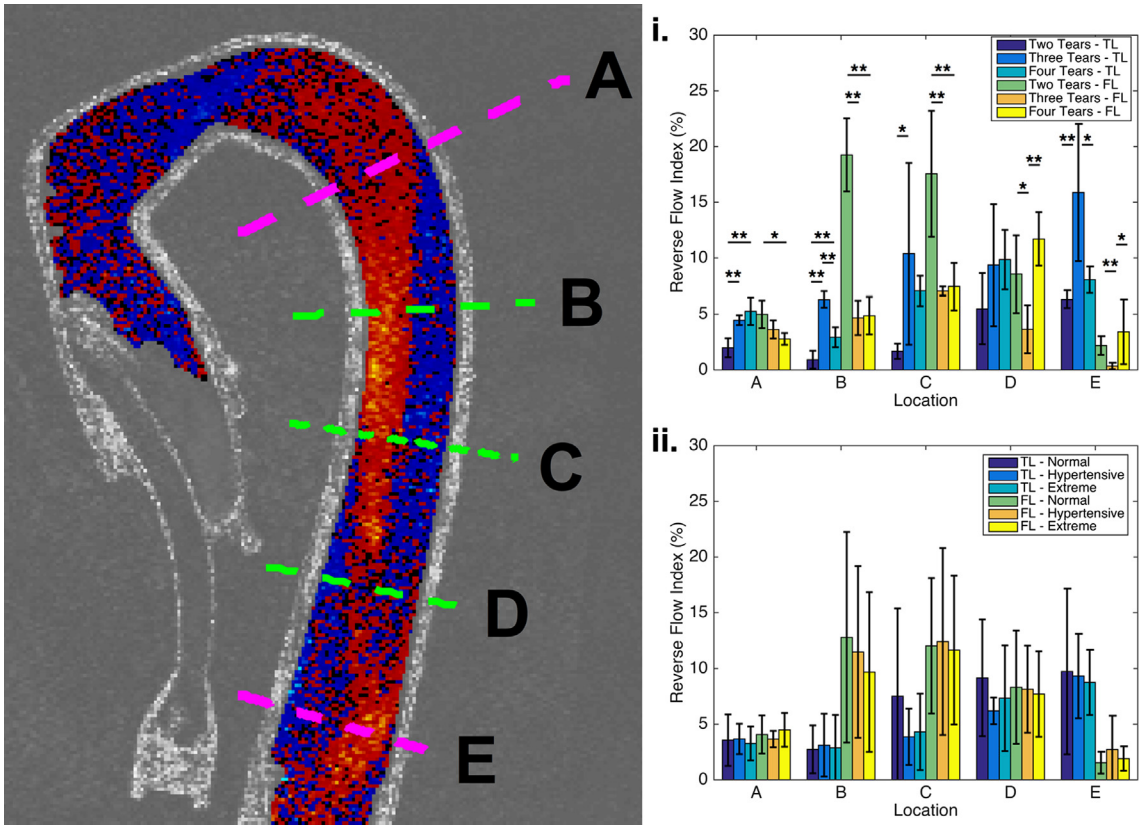

Fig. 5. Differences in RFI calculated across varying pressure and tear conditions at locations seen on left. When aggregated across pressure conditions, significant differences in RFI are found between different tear numbers (**i**). However, when aggregated across tear number, significant differences are washed out (**ii**). (* denotes $p < 0.05$, ** denotes $p < 0.01$).

Table 1
Reverse flow index calculated across varying dissection anatomies, all values in %. TL – true lumen, FL – false lumen.

Location	Two tears		Three tears		Four tears	
	TL	FL	TL	FL	TL	FL
Entry	1.99	4.99	4.46	3.64	5.26	2.79
25%	0.924	19.2	6.31	4.67	2.94	4.87
50%	1.68	17.5	10.4	7.05	7.06	7.45
75%	5.48	8.56	9.38	3.65	9.59	11.7
Exit	6.33	2.19	15.9	0.350	8.06	3.43

Ultimately, the anatomy of aortic dissection, in particular the configuration of intimal flap tears, strongly influences the hemodynamics seen with this condition. Small changes in the intimal flap may significantly alter the fluid flow and cardiac efficiency, and portend differences in outcomes, as reported clinically (Onitsuka et al., 2004; Tolenaar et al., 2013; Tolenaar et al., 2013; Tsai et al., 2008; Ueki et al., 2014). Furthermore, the relationship between siphoning branch vessels and intimal tears may have an important impact on false lumen flows as well as the need for thrombosis of this lumen. Recent work has shown, for example, that proximity of the primary entry tear to the left subclavian artery may aid in directing flow into the false lumen (Pirola et al., 2019), while visceral branches may alter flow in the distal false lumen.

While pressure control is a cornerstone of the management of patients with aortic dissection, it does not appear to have an effect on flow patterns in the vessel, as per the initial hypothesis. This is corroborated by fluid mechanics theory, which indicates that fluid flow is driven by spatial gradients in pressure between the heart and legs, as opposed to absolute pressure or temporal pressure gradients (Pfitzner, 1976; Sutera and Skalak, 1993). It is important to note that only small pressure gradients on the order of a few millimeters of mercury are required to drive blood flow through the arteries. Thus, we may consider the pressure at a fixed location, such as a standard blood pressure reading, to be decoupled from flow rate and other flow phenomena. This eases requirements for experimental study, as a single pressure regime may be used. However, it indicates that static pressure does not drive complex flow phenomena.

Alternatively, pressure may play a role in the solid mechanics of the aorta, as increased pressure increases vascular wall tension and tensile stresses, as opposed to shear stresses. Cyclic tensile stress concentrations may contribute to weakening and eventual failure of the wall, corresponding to aneurysmal degeneration and rupture, respectively. In addition, the decreased thickness of aortic wall of the false lumen contributes to a greater hoop stress. As a

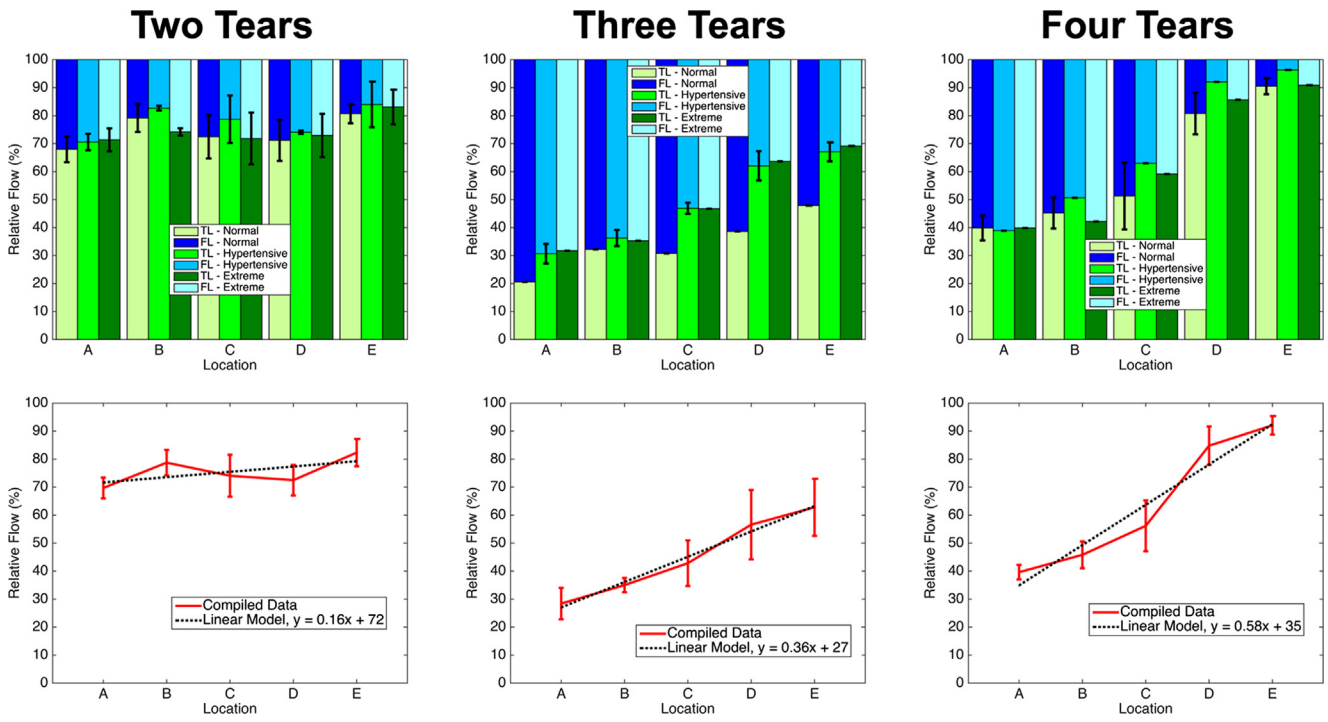

Fig. 6. Increase in relative true lumen flow along length of dissection in the presence of fenestrations. Note no change in relative flows when no intermediate fenestrations are present.

Table 2
Maximum true and false lumen velocities, all values in cm/s. TL – true lumen, FL – false lumen.

Location	Two tears		Three tears		Four tears	
	TL	FL	TL	FL	TL	FL
Entry	22.5 ± 2.3	3.18 ± 2.0	15.6 ± 5.7	3.67 ± 2.5	19.5 ± 5.1	4.52 ± 3.2
25%	37.5 ± 6.4	4.43 ± 3.8	32.8 ± 4.6	7.50 ± 1.4	34.4 ± 2.5	5.01 ± 3.9
50%	40.4 ± 8.5	5.17 ± 3.9	32.6 ± 5.4	4.7 ± 1.4	31.0 ± 6.3	6.10 ± 1.7
75%	36.4 ± 5.1	2.73 ± 2.7	29.0 ± 3.7	4.70 ± 1.2	39.1 ± 12	7.05 ± 3.2
Exit	30.4 ± 3.0	2.84 ± 2.9	28.1 ± 3.9	4.49 ± 4.4	29.8 ± 2.4	4.05 ± 2.0

Table 3
P-values for one-way analysis of variance testing of true lumen flow rates (Q_T) and splits (Q_T/Q_{tot}) for varying pressure conditions.

Location	Two tears		Three tears		Four tears	
	Q_T	$\frac{Q_T}{Q_{tot}}$	Q_T	$\frac{Q_T}{Q_{tot}}$	Q_T	$\frac{Q_T}{Q_{tot}}$
Entry	0.550	0.658	0.277	0.359	0.990	0.983
25%	0.0182	0.173	0.482	0.653	0.765	0.675
50%	0.526	0.670	0.243	0.140	0.818	0.762
75%	0.610	0.883	0.202	0.244	0.502	0.625
Exit	0.989	0.803	0.240	0.193	0.00731	0.498

Table 4
P-values for one-way analysis of variance testing of true and false lumen reverse flow index for varying pressure conditions. TL – true lumen, FL – false lumen.

Location	Two tears		Three tears		Four tears	
	TL	FL	TL	FL	TL	FL
Entry	0.906	0.737	0.895	0.371	0.820	0.779
25%	0.934	0.229	0.630	0.0732	0.0437	0.906
50%	0.133	0.783	0.0478	0.0444	0.403	0.965
75%	0.707	0.732	0.123	0.378	0.0325	0.401
Exit	0.634	0.310	0.256	0.746	0.203	0.195

result, further study of the solid mechanics of this pathology is warranted.

The diagnosis of aortic dissection is commonly followed with anatomic imaging, namely computed tomography. In the future, 4D PCMR may be used to characterize the functional status of the aorta with regards to flow as well as anatomy, which may be of use for individual patient prognosis and in deciding on the use of endovascular intervention. Future correlation between the observed flow perfusion pathways, flow reversal, and luminal thrombosis may help solidify this indication for flow imaging. In addition, fluid vortices may be used to identify locations of fenestrations as a critical landmark for endovascular repair unavailable with standard anatomic imaging. Previous investigation has found CT to be insufficient for identification of tear sites due to limitations in resolution and orientation (Dinsmore et al., 1986; Nienaber et al., 1993). Similar difficulties arise with the use of both transthoracic and transesophageal echocardiography (Nienaber et al., 1993). However, with direct visualization of vertical and jet-like structures with 4D flow MR imaging, tears may be easily identified using this modality.

4.1. Limitations

Due to technical challenges in the fabrication process, aortic branches were not included in this model. While these will have an impact on the resulting fluid mechanics, flow conditions were matched to inlet conditions beyond the cephalic vessels to approximate gross fluid dynamics alterations. Further, the working fluid used (water), has a kinematic viscosity that is different from that of the blood, resulting in different fluid dynamics conditions, as dictated by the physical limitations of the flow setup. However, two critical non-dimensional fluid mechanics parameters, the Reynolds and Womersley numbers, were calculated to be on the same of order of magnitude as those of natural aortic blood flow (Reynolds – 1460 vs. 1630, Womersley – 14 vs. 17), and no transitions to turbulence were observed.

5. Conclusions

Dissections of the descending aorta present a complex anatomic challenge to the surgeon. We demonstrated that a model of aortic dissection mimics flow patterns seen *in vivo* between the true and false lumen. As hypothesized, intermediate fenestrations were found to reduce false lumen flow reversal. Our quantitative measurements of velocity in models of dissections illustrate the vortical flow patterns set up by tears between the true and false lumen. The vortices are observed prominently at each tear and cause blood to communicate both into and out of the false lumen. Distal tears were most easily visualized via velocity imaging, which revealed transverse fluid flow and vortices accompanying these fenestrations. In contrast, high arterial pressure per se did not have an effect on the fluid dynamics of the dissected aorta. Future work is aimed at characterizing the influence of other anatomic parameters, such as the size of the entry tear, on aortic dissection fluid mechanics.

Acknowledgments

We would like to thank Mark Young of Medtronic, Inc. for his work towards this project. In addition, we acknowledge funding support for this project from Medtronic, Inc.

Declaration of Competing Interest

Birjiniuk – Medtronic, Inc.: graduate research assistantship.
Veeraswamy – Medtronic, Inc: consulting fees, grant support.
Oshinski – None.
Ku – None.

References

Ahrens, J., Geveci, B., Law, C., 2005. ParaView: an end-user tool for large data visualization. In: Hansen, C.D., Johnson, C.R. (Eds.), Visualization Handbook. Academic Press, Cambridge, pp. 717–731.
Akhtar, R., Schwarzer, N., Sherratt, M.J., Watson, R.E.B., Graham, K., Trafford, A.W., et al., 2009. Nanoindentation of histological specimens: mapping the elastic properties of soft tissues. J. Mater. Res. 24 (3), 638–646.
Akutsu, K., Nejima, J., Kiuchi, K., Sasaki, K., Ochi, M., Tanaka, K., et al., 2004. Effects of the patent false lumen on the long-term outcome of type B acute aortic dissection. Eur. J. Cardio-thorac. 26, 359–366.
Barker, A.J., van Ooij, P., Bandi, K., Garcia, J., Albaghdadi, M., McCarthy, P., et al., 2014. Viscous energy loss in the presence of abnormal aortic flow. Magn. Reson. Med. 72, 620–628.
Berguer, R., Parodi, J.C., Schlicht, M., Khanafer, K., 2015. Experimental and clinical evidence supporting septectomy in the primary treatment of acute Type B thoracic aortic dissection. Ann. Vasc. Surg. 29, 167–173.
Birjiniuk, J., Timmins, L.H., Young, M., Leshnower, B.G., Oshinski, J.N., Ku, D.N., et al., 2017. Pulsatile flow leads to intimal flap motion and flow reversal in an *in vitro* model of Type B aortic dissection. Cardiovasc. Eng. Tech. 8 (3), 378–389.
Blount, K.J., Hagspiel, K.D., 2009. Aortic diameter, true lumen, and false lumen growth rates in chronic Type B aortic dissection. Am. J. Roentgenol. 192, W222–W229.
Casas, B., Lantz, J., Dyverfeldt, P., Ebbers, T., 2016. 4D flow MRI-based pressure loss estimation in stentotic flows: evaluation using numerical solutions. Magn. Reson. Med. 75, 1808–1821.
Characteristic Properties of Silicone Rubber Compounds. Shin-Etsu Co. (Last accessed December 12, 2018). <http://www.silicone.jp/e/catalog/pdf/rubber_e.pdf>.
Cheng, Z., Juli, C., Wood, N.B., Gibbs, R.G.J., Xu, X.Y., 2014a. Predicting flow in aortic dissection: comparison of computational model with PC-MRI velocity measurements. Med. Eng. Phys. 36, 1176–1184.
Cheng, Z., Wood, N.B., Gibbs, R.G.J., Xu, X.Y., 2014b. Geometric and flow features of type B aortic dissection: initial findings and comparison of medically treated and stented cases. Ann. Biomed. Eng. 43, 177–189.
Clough, R.E., Nienaber, C.A., 2015. Management of acute aortic syndromes. Nat. Rev. Cardiol. 12, 103–114.
Clough, R.E., Waltham, M., Giese, D., Taylor, P.R., Schaeffter, T., 2012. A new imaging method for assessment of aortic dissection using four-dimensional phase contrast magnetic resonance imaging. J. Vasc. Surg. 55, 914–923.
Clough, R.E., Zymvragoudakis, V.E., Biasi, L., Taylor, P.R., 2014. Usefulness of new imaging methods for assessment of type B aortic dissection. Ann. Cardiothorac. Surg. 3, 314–318.
Dinsmore, R.E., Wedeen, V.J., Miller, S.W., Rosen, B.R., Fifer, M., Vlahakes, G.J., et al., 1986. MRI of dissection of the aorta: recognition of the intimal tear and differential flow velocities. Am. J. Roentgenol. 146 (6), 1286–1288.
Dyverfeldt, P., Hope, M.D., Tseng, E.E., Saloner, D., 2013. Magnetic resonance measurement of turbulent kinetic energy for the estimation of irreversible pressure loss in aortic stenosis. JACC-Cardiovasc. Imag. 6 (1), 64–71.
Evangelista, A., Salas, A., Ribera, A., Ferreira-González, I., Cuellar, H., Pineda, V., et al., 2012. Long-term outcome of aortic dissection with patent false lumen: predictive role of entry tear size and location. Circulation 125, 3133–3141.
François, C.J., Markl, M., Schiebler, M.L., Niespodzany, E., Landgraf, B.R., Schlensak, C., et al., 2013. Four-dimensional, flow-sensitive magnetic resonance imaging of blood flow patterns in thoracic aortic dissections. J. Thorac. Cardiov. Sur. 145 (5), 1359–1366.
Guzzardi, D.G., Barker, A.J., van Ooij, P., Malaisrie, S.C., Puthumana, J.J., Belke, D.D., et al., 2015. Valve-related hemodynamics mediate human bicuspid aortopathy: insights from wall shear stress mapping. J. Am. Coll. Cardiol. 66, 892–900.
Haskett, D., Johnson, G., Zhou, A., Utzinger, U., Vande, Geest J., 2010. Microstructural and biomechanical alterations of the human aorta as a function of age and location. Biomech. Model. Mech. 9 (6), 725–736.
Hope, T.A., Markl, M., Wigström, L., Alley, M.T., Miller, D.C., Herfkens, R.J., 2007. Comparison of flow patterns in ascending aortic aneurysms and volunteers using four-dimensional magnetic resonance velocity mapping. J. Magn. Reson. Imag. 26, 1471–1479.
Karmonik, C., Partovi, S., Müller-Eschner, M., Bismuth, J., Davies, M.G., Shah, D.J., et al., 2012. Longitudinal computational fluid dynamics study of aneurysmal dilatation in a chronic DeBakey type III aortic dissection. J. Vasc. Surg. 56, 260–263.
Kilner, P.J., Yang, G.Z., Mohiaddin, R.H., Firmin, D.N., Longmore, D.B., 1993. Helical and retrograde secondary flow patterns in the aortic arch studied by three-directional magnetic resonance velocity mapping. Circulation 88 (5), 2235–2247.
Kumar, V., Abbas, A.K., Fausto, N., Aster, J.C., 2009. Robbins and Cotran Pathologic Basis of Disease. Saunders.
LeMaire, S.A., Russell, L., 2011. Epidemiology of thoracic aortic dissection. Nat. Rev. Cardiol. 8 (2), 103–113.
Markl, M., Frydrychowicz, A., Kozerke, S., Hope, M., Wieben, O., 2012. 4D Flow MRI. J. Magn. Reson. Imag. 36, 1015–1036.

Menichini, C., Xu, X.Y., 2016. Mathematical modeling of thrombus formation in idealized models of aortic dissection: initial findings and potential applications. J. Math. Biol. 73 (5), 1205–1226.
Menichini, C., Cheng, Z., Gibbs, R.G.J., Xu, X.Y., 2017. Predicting false lumen thrombosis in patient-specific models of aortic dissection. J. R. Soc. Interf. 13, 20160759.
Nienaber, C.A., Kische, S., Rousseau, H., Eggebrecht, H., Rehders, T.C., Kundt, G., et al., 2013. Endovascular repair of Type B aortic dissection: long-term results of the randomized investigation of stent grafts in aortic dissection trial. Circ-Cardiovasc. Int. 6, 407–416.
Nienaber, C.A., Rousseau, H., Eggebrecht, H., Kische, S., Fattori, R., Rehders, T.C., et al., 2009. Randomized comparison of strategies for Type B aortic dissection: the INvestigation of STEnt grafts in Aortic Dissection (INSTEAD) trial. Circulation 120, 2519–2528.
Nienaber, C.A., von Kodolitsch, Y., Nicolas, V., Siglow, V., Piepho, A., Brockhoff, C., et al., 1993. The diagnosis of thoracic aortic dissection by noninvasive imaging procedures. New Engl. J. Med. 328 (1), 1–9.
Onitsuka, S., Akashi, H., Tayama, K., Okazaki, T., Ishihara, K., Hiromatsu, S., et al., 2004. Long-term outcome and prognostic predictors of medically treated acute type B aortic dissections. Ann. Thorac. Surg. 78, 1268–1273.
Pfitzner, J., 1976. Poiseuille and his law. Anaesthesia 31, 273–275.
Pirola, S., Guo, B., Menichini, C., Saitta, S., Fu, W., Dong, Z., et al., 2019. 4D flow MRI-based computational analysis of blood flow in patient-specific aortic dissection. IEEE T. Bio-Med. Eng.
Stalder, A.F., Russe, M.F., Frydrychowicz, A., Bock, J., Hennig, J., Markl, M., 2008. Quantitative 2D and 3D phase contrast MRI: optimized analysis of blood flow and vessel wall parameters. Magn. Reson. Med. 60, 1218–1231.
Sueyoshi, E., Sakamoto, I., Uetani, M., 2009. Growth rate of affected aorta in patients with Type B partially closed aortic dissection. Ann. Thorac. Surg. 88, 1251–1257.
Sutera, S.P., Skalak, R., 1993. The history of Poiseuille's Law. Annu. Rev. Fluid Mech. 25, 1–20.
Tolenaar, J.L., van Herwaarden, J.A., Verhagen, H., Moll, F.L., Muhs, B.E., Trimarchi, S., 2013. Importance of entry tears in type B aortic dissection prognosis. Ann. Cardiothorac. Surg. 2, 631–632.
Tolenaar, J.L., van Keulen, J.W., Jonker, F.H.W., van Herwaarden, J.A., Verhagen, H.J. M., Moll, F.L., et al., 2013. Morphologic predictors of aortic dilatation in type B aortic dissection. J. Vasc. Surg. 58, 1220–1225.
Tolenaar, J.L., van Keulen, J.W., Trimarchi, S., Jonker, F.H.W., van Herwaarden, J.A., Verhagen, H.J.M., et al., 2013. Number of entry tears is associated with aortic growth in type B dissections. Ann. Thorac. Surg. 96, 39–42.
Tsai, T.T., Evangelista, A., Nienaber, C.A., Myrmel, T., Meinhardt, G., Cooper, J.V., et al., 2007. Partial thrombosis of the false lumen in patients with acute type B aortic dissection. New Engl. J. Med. 357, 349–359.
Tsai, T.T., Schlicht, M.S., Khanafer, K., Bull, J.L., Valassis, D.T., Williams, D.M., et al., 2008. Tear size and location impacts false lumen pressure in an ex vivo model of chronic type B aortic dissection. J. Vasc. Surg. 47 (4), 844–851.
Ueki, C., Sakaguchi, G., Shimamoto, T., Komiya, T., 2014. Prognostic factors in patients with uncomplicated acute type B aortic dissection. Ann. Thorac. Surg. 97, 767–773.
Williams, D.M., Lee, D.Y., Hamilton, B.H., Marx, M.V., Narasimham, D.L., Kazanjian, S. N., et al., 1997. The dissected aorta: percutaneous treatment of ischemic complications – principles and results. J. Vasc. Int. Rad. 8, 605–625.